Nanochem Res 6(1): 104-116, Winter and Spring 2021

RESEARCH PAPER

Synthesis of nickel oxide/gadulinium doped ceria nanostructures by new methods as anode material for solid oxide fuel cells: Ni(II) complexes as new precursors

Somayeh Ghamari Arbati, Maryam Ranjbar*

Department of Chemical Technologies, Iranian Research Organization for Science and Technology (IROST) , Tehran, Iran

ARTICLE INFO

Article History:
Received 17 December 2020
Accepted 28 January 2021
Published 15 March 2021

Keywords:
Anode
Morphology
Catalytic activity
Solid oxide fuel cell
Sol-gel

ABSTRACT

Nickel oxide/gadolinium dopped ceria nano powders, NiO/GDC, (NGC) with controlled morphology were synthesized by the sol-gel method. The nickel(II) coordination compounds have been used as new precursors for the preparation of ceramic materials, NiO/GDC, as anodic powders for application in solid oxide fuel cells. The formation of diverse morphologies with different porosity was observed by varying the Nickel(II) coordination compounds, $[NiL^2(\mu\text{-acetylenedicarboxylate})]_n$, $[NiL^2(\mu\text{-terephthalate})]_n$ and $[NiL^2(\mu\text{-2,6 pyridinedicarboxylate})]_n$. Then three different kinds of nickel oxide / gadolinium dopped ceria, namely NGC (a), NGC (b), and NGC (c) samples, each of a different shape, were developed by new precursors. These powders have been used as electrocatalysts for solid oxide fuel cells. The catalytic performance of NGC anodes for the hydrogen oxidation reaction was analyzed via impedance spectra test using yttria-stabilized zirconia (YSZ)-supported symmetry half-cell. The modified NGC (c) anode powder fabricated with the new precursor of $[NiL^2(\mu\text{-2,6 pyridinedicarboxylate})]_n$ (N'-(pyridine-3-yl)methylene)isonicotinohydrazide (L)) manifested the least polarization resistivity of 0.106 Ω. cm^2 measured at 800 under humidified H_2. The NGC (c) anode powder with a better pore distribution and excellent microstructure demonstrated the most desirable electro-catalytic activity.

How to cite this article
Ghamari Arbati S., Ranjbar M. Synthesis of nickel oxide/gadulinium doped ceria nanostructures by new methods as anode material for solid oxide fuel cells: Ni(II) complexes as new precursors . Nanochem Res, 2021; 6(1):104-116. DOI: 10.22036/ncr.2021.01.010

INTRODUCTION

The anodes of solid oxide fuel cells (SOFCs) can be classified in terms of temperature, electrode polarization, conductivity and structure each of which affects their efficiency and properties [1]. NiO/GDC cermets as anode materials for SOFCs have received particular attention, considering their high electrochemical activity and stability at relatively high temperatures (600-800 °C) [2-6]. NiO/GDC cermets are usually prepared by mixing NiO (catalyst) and GDC powder as a supporting network for the Ni catalyst. The electrochemical reaction value is equal to the length of the triple-phase boundaries (TPBs), which also depends on the microstructure of NiO/GDC cermets [2]. The morphology of a complex has a significant effect on the catalytic activity. In addition, it is often reported that the modification of morphology by various techniques has a great impact on the performance of solid oxide fuel cells [7-10]. Thus, it is essential to control the structure of the NiO/GDC anode material. Research activities have been undertaken on the morphology and microstructure manipulation of the NiO/GDC by using oxalyl dihydrazide (ODH) and hexamethylnetetramine

* Corresponding Author Email: *marandjbar@irost.ir (M.Ranjbar).*

(HMT) [11]. In another study, nanocrystalline NiO/GDC powder was modified by the application of Na-Alginate as the effective agent in the ionic sol-gel method [12]. The synthesis of two new nanoparticles of copper(II) and nickel(II) complexes with Schiff base ligand also demonstrated the Schiff base complexes may be suitable precursors for the preparation of nanoscale materials with different morphologies [13]. The porosity, thermal stability and electrochemical behavior of the modified NiO-GDC are compared with the conventional NiO-GDC prepared by nickel nitrate salt as previously reported [14]. In the current study, the effects of Nickel coordination compounds as precursors on the microstructure of NiO/GDC anode powders were explored. Three Nickel coordination compounds with N'-(pyridine-3-yl)methylene)isonicotinohydrazide (L), containing anions acetylenedicarboxylate, $[NiL^2(\mu\text{-acetylenedicarboxylate})]_n$, terephthalate, $[NiL^2(\mu\text{-terephthalate})]_n$, and 2,6-pyridinedicarboxylate, $[NiL^2(\mu\text{-2,6 pyridinedicarboxylate})]_n$ were synthesized. Eventually, three NiO/GDC (NGC) anode powders with $[NiL^2(\mu\text{-acetylenedicarboxylate})]_n$ complex, NGC (a) powder, $[NiL^2(\mu\text{-terephthalate})]_n$ complex, NGC (b) powder, and $[NiL^2(\mu\text{- 2,6 pyridinedicarboxylate})]_n$, NGC (c) powder were synthesized. Later, we investigated the electrical attributes of NGC powders by impedance electrochemical spectroscopy (IES). Impedance results showed that morphology had a dramatic influence on the electrical performance of NiO/GDC anodes, and the entire developed cermets portrayed enhanced electrical performance. Among these compared samples, the NGC (c) anode powder with a better morphology presented the best electro-catalytic activity.

EXPERIMENTAL PROCEDURE

The N'-(pyridine-3-yl)methylene)isonicotinohydrazide, Schiff base (L), was prepared according to the method reported by Ni and co-workers (2009) [15]. The reaction of 3-pyridinecarboxaldehyde with isonicotinohydrazide in ethanol solvent at room temperature leads to the formation of a Schiff base (L). For the synthesis of $[NiL^2(\mu\text{-acetylenedicarboxylate})]_n$, $[NiL^2(\mu\text{-terephthalate})]_n$ and $[NiL^2(\mu\text{-2,6pyridinedicarboxylate})]_n$, in addition to the Schiff base (L), the acetylenedicarboxylic acid, terephthalic acid, and 2,6-pyridinedicarboxylic acid ligands were used, respectively. This solution was transferred into a thermal bomb for 72 hours at 170°C. The resulting precipitate was isolated and rinsed with ethanol and distilled water, respectively. The molecular structure of the Nickle complexes is shown in Fig. 1. Next, the developed structures were identified with the techniques of FT-IR (Bruker tensor 27 spectrometers), Raman (dectris Eiger X9M area detector) and diffuse reflection spectroscopy (DRS) (shimadzu spectrophotometer-Japan). The flow chart demonstrating the production process of the NGC powders using the sol-gel procedure is illustrated in Fig. 2. In the synthesis of NGC powders, after generating a homogeneous solution, the solution's temperature was set to 90 °C for the extraction of excess water. The resulting gels were dried at 110 °C and further calcined at 800 °C. Eventually, NGC

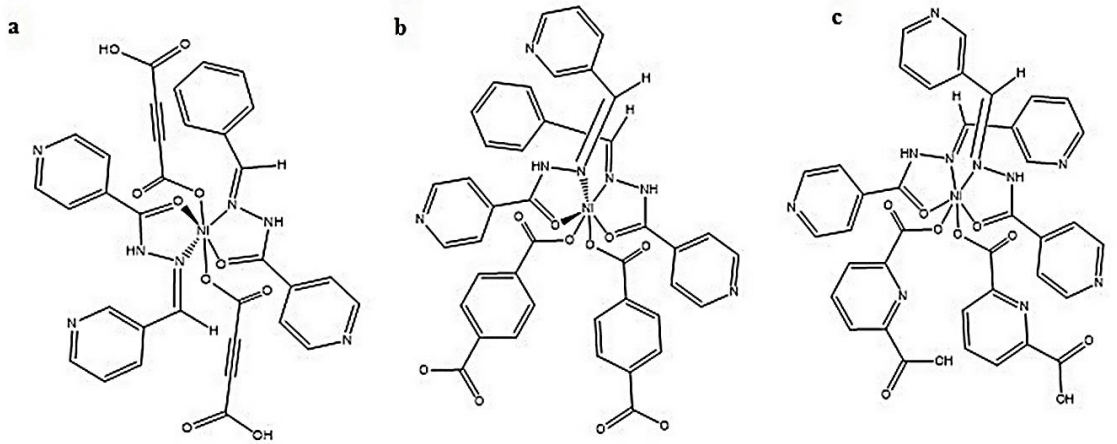

Fig. 1. The molecular structure of the a) $[NiL^2(\mu\text{-acetylenedicarboxylate})]_n$, b) $[NiL^2(\mu\text{-terephthalate})]_n$ and c) $[NiL^2(\mu\text{-2,6 pyridinedicarboxylate})]_n$

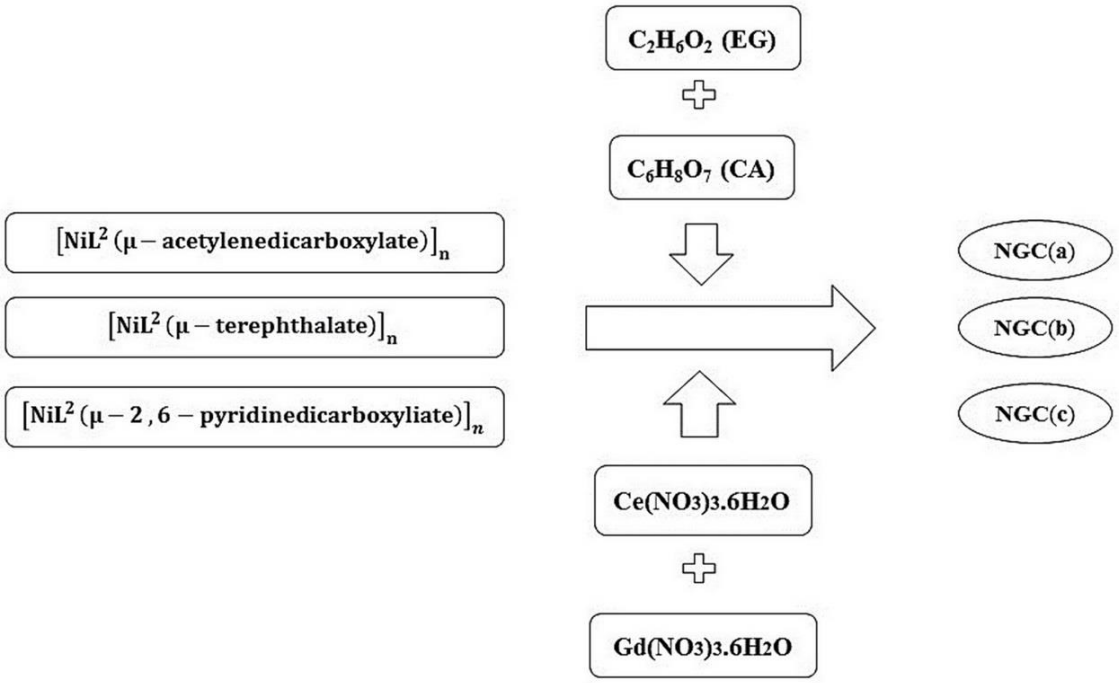

Fig. 2. The flow chart for the synthesis of the NGC powders using a sol-gel method

(a), NGC (b), and NGC (c) samples, each of a different shape, were developed by new precursors. Characterization of the produced powders was carried out by X-ray diffraction (XRD) (EQuniox 3000 STOE-STADV). The powders were also analyzed by TGA (PL-STA 1500), in Argon gas at 25–800 °C at a heating rate of 10 °C/min. The morphology of the manufactured complexes was done by scanning electron microscopy/ energy-dispersive (SEM, JEOL 6460 LV). The specific surface area of the developed powder was estimated by BET (Brunauer, Emmett, Teller) analysis (BELSORB-mini II). The electro-catalytic activity of the NGC anodes was characterized by the electrochemical impedance spectroscopy (EIS) technique (PARSTAT 2273 potentiostat/ galvanostat), and YSZ electrolyte supported symmetrical half-cell, which was similar to that reported in another study [16]. The electrolyte discs were prepared by die-pressing 8 mol % Y_2O_3–ZrO_2 powder (YSZ, Tosoh, Japan), followed by sintering at 1500 °C for 4 h. The diameter and thickness of the electrolyte were 19 and 0.9 mm, respectively. The surface of the electrolyte pellets was roughened by grinding it with sandpaper to increase the contact between the electrode and electrolyte. The conventional and modified NiO-GDC powders were mixed with an ink vehicle (Fuel cell Materials, USA), and applied to the YSZ pellets by the slurry painting method; this was followed by sintering at 1380 °C for 2 h in air. The electrode area was 0.4 cm^2 after sintering. A Pt paste was applied as the counter and reference electrodes. The electrochemical performance of the cermet anodes was characterized by the electrochemical impedance spectroscopy (EIS) technique in the frequency range of 0.1 Hz to 0.1 MHz and signal amplitude of 10 mV. The EIS spectra were recorded at 650-800 °C with 50 °C intervals using wet hydrogen/nitrogen (50:50 vol. ratio) gas as the fuel and ambient air as the oxidant. The impedance response of the modified NiO-GDC anodes was measured and compared.

RESULTS AND DISCUSSION

According to the Schiff base's IR spectrum (L) (Fig. 3a), the band present at 1679 cm^{-1} denotes the imine group (C=N). The presence of imine group band in 1679 cm^{-1} indicates the formation of a Schiff base. Furthermore, the absorption band at 3301 cm^{-1} is attributed to the N-H stretching vibrations. The stretching vibration bands of N-H indicates the absence of tautomerization enol-ketone of ligand, and the Schiff base is a ketone

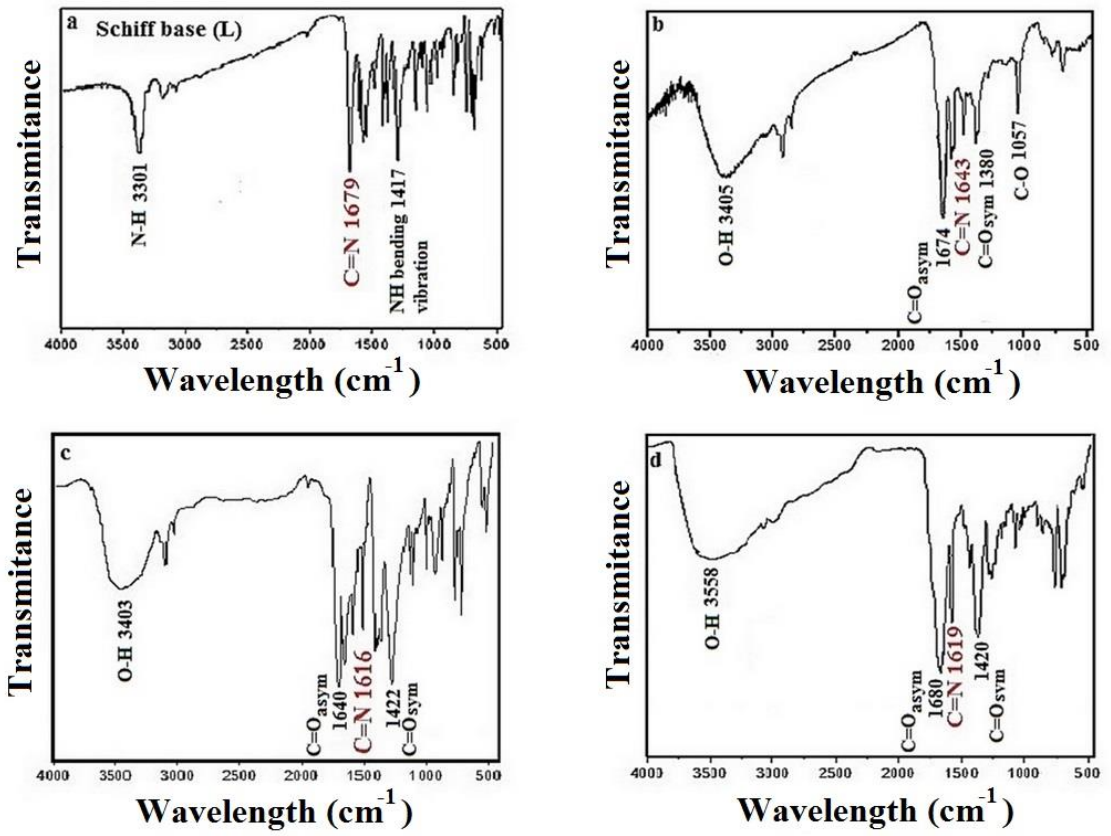

Fig. 3. FTIR spectra of a) Schiff base, b) $[NiL^2(\mu\text{-acetylenedicarboxylate})]_n$, c) $[NiL^2(\mu\text{-terephthalate})]_n$ and d) $[NiL^2(\mu\text{-2,6 pyridinedicarboxylate})]_n$

form. In the IR spectrum of Nickel complexes (Fig. 3b-d) synthesized by Schiff base (L) and acetylenedicarboxylic acid, terephthalic acid and 2,6-pyridinedicarboxylic acid ligands, the absorption band of imine group (C=N) is seen at lower frequencies. This shift towards lower frequencies represents the coordination of the ligand to the metal, and synthesis of the Schiff base (L) is approved. In the low energy band scope of IR complexes, a series of absorption peaks (1400-1600 cm^{-1}) is observed, attributed to the pyridine ring. Moreover, ionic carboxylates depict two bands (νCOO_{asym} and νCO_{sym}) within their spectra. In the IR complexes (Fig. 3b-d), strong absorptions in the region 1690-1820 cm^{-1} and weaker absorptions around 1396-1420 cm^{-1} are typical of the asymmetric stretching behavior of the carboxylate group and symmetric carboxylate stretching mode, respectively [17]. The separation of the bands$\Delta\ \nu = (\nu CO_{asym} - \nu CO_{sym})$ also indicates the structure of the given carboxylate. Compared to the stretching frequencies of free or uncoordinated carboxylate ions, in this case the asymmetric and symmetric stretching frequencies of the carbonyl groups change.; a broad splitting of the COO stretching frequencies ($\Delta\nu$) usually indicates the presence of monodentate coordination in a metal carboxylate [17, 18]. Therefore, the dicarboxylate bridge in all Nickel complexes is attached monodentately to the metal. The assigned peak of the C=N band at 1679 cm^{-1} of the Raman spectrum of the Schiff base (L) (Fig. 4a), shifts to lower frequencies in the Ni complexes (Fig. 4b-d). Moreover, in Fig 4b-d the type and location of the most important functional groups of Nickel complexes in the Raman spectra have been illustrated, which are in good agreement with the IR spectrum of Schiff base (L). Fig. 5 shows the results of the absorption spectra for the Ni complexes which were carried out by diffuse reflection spectroscopy (DRS). The maximum absorption for Ni complexes observed in the DRS is listed in Table 1. The charge transfer such as LMCT usually appears in the highest energy region of the DRS spectra. Furthermore, along the DRS spectra

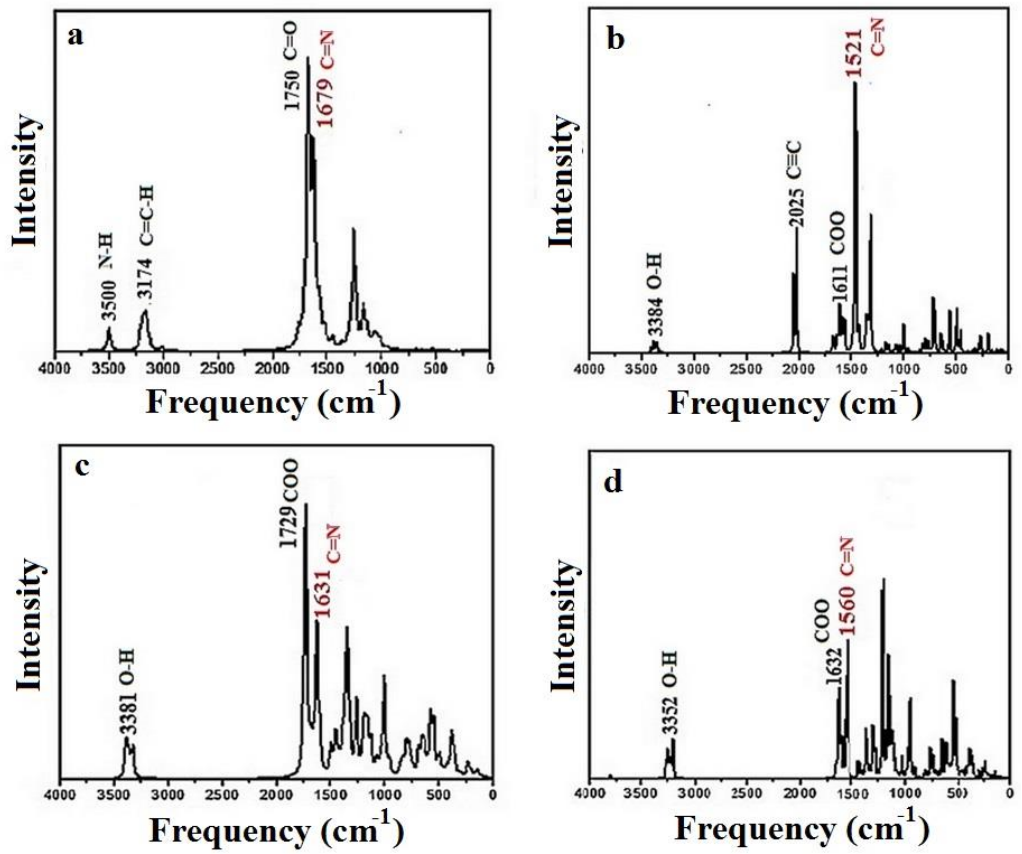

Fig. 4. Raman spectra of a) Schiff base, b) $[NiL^2(\mu\text{-acetylenedicarboxylate})]_n$, c) $[NiL^2(\mu\text{-terephthalate})]_n$ and d) $[NiL^2(\mu\text{-2,6 pyridinedicarboxylate})]_n$

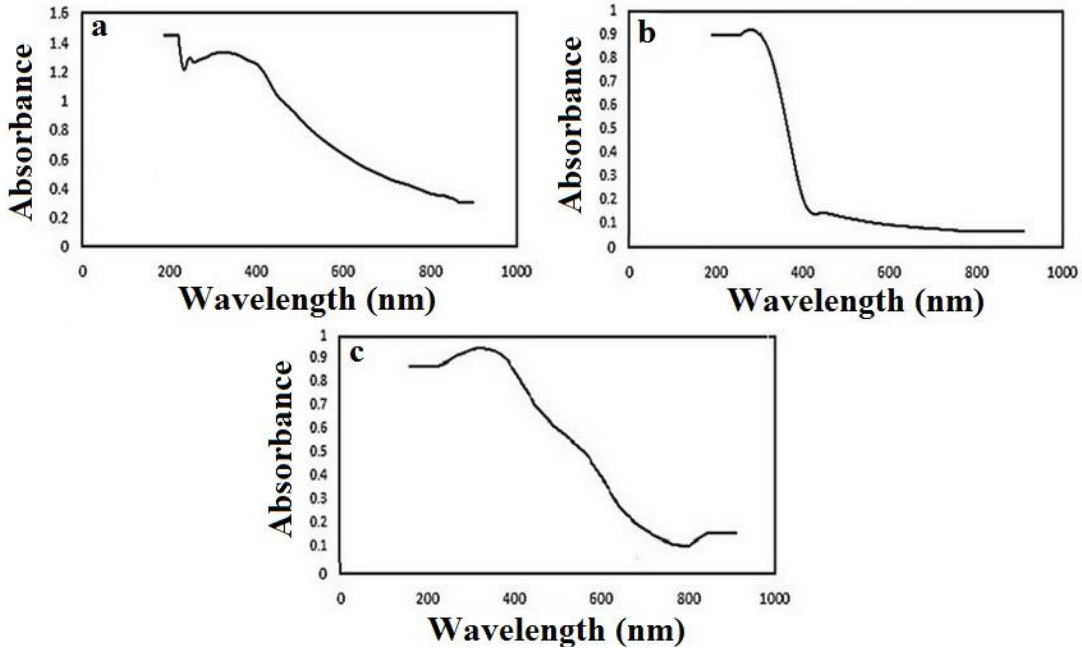

Fig. 5. DRS spectra of the a) $[NiL^2(\mu\text{-acetylenedicarboxylate})]_n$, b) $[NiL^2(\mu\text{-terephthalate})]_n$ and c) $[NiL^2(\mu\text{-2,6 pyridinedicarboxylate})]_n$

Table 1. The most essential adsorption bands of the a) $[NiL^2(\mu\text{-acetylenedicarboxylate})]_n$, b) $[NiL^2(\mu\text{-terephthalate})]_n$ and c) $[NiL^2(\mu\text{-2,6 pyridinedicarboxylate})]_n$ in the DRS spectroscopy

	Wavelength /nm	Abs.
a	328	1.334
	250	1.295
	258	1.266
	236	1.215
b	278	0.926
	444	0.144
	426	0.14
	796	0.066
c	344	0.92
	794	0.14

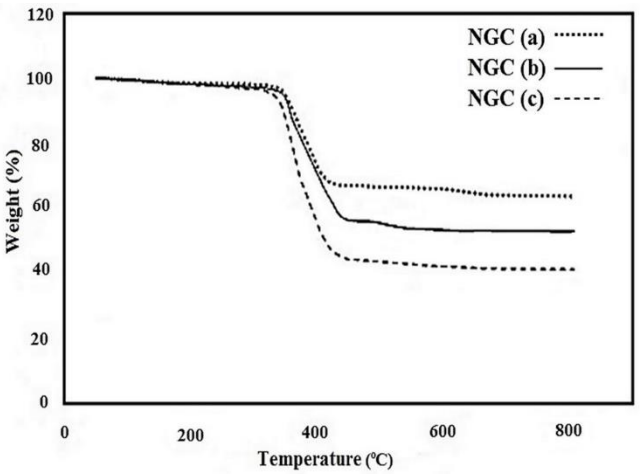

Fig. 6. TG/DTG diagram of the a) NGC (a), b) NGC (b) and c) NGC (c)

in the lower energy region (visible region), other bands can be seen to be formed in response to the d-d transitions which are weaker than the LMCT transition. Fig. 6 demonstrates the thermogravimetric analysis (TGA) of the NGC (a), (b) and (c) powders with three major weight loss stages as observed from the TGA plots. The first weight loss step occurred in all samples corresponding to the dehydration of the samples due to the presence of water molecule and free ethylene glycol [19]. The second decrease in weight loss occurs due to the decomposition of Nickel coordination compounds. According to Fig. 6 and by comparing the TGA plots, it is indicated that due to the application of a Nickel complex with higher weight, the weight of the developed NGC (c) composite was also increased. However, the NGC (a) due to the use of Nickel complex with a lower weight manifested a lower weight loss value. Finally, the last step for all samples is to remove any remaining organic material and nitrate. The XRD patterns of the NGC powders calcined at 800 °C for 2h are portrayed in Fig. 7. In the XRD patterns, there were no signs of a secondary impurity phase. The peaks for the entire samples perfectly matched with cubic NiO (Fm3m) and cubic GDC (Fm3m). The NGC (a), (b), and (c) powders show all main reflections, which are in accordance with the reported literature [20, 21]. The crystallite sizes of NiO and GDC phases in NGC (a), (b) and (c) anode powders were calculated

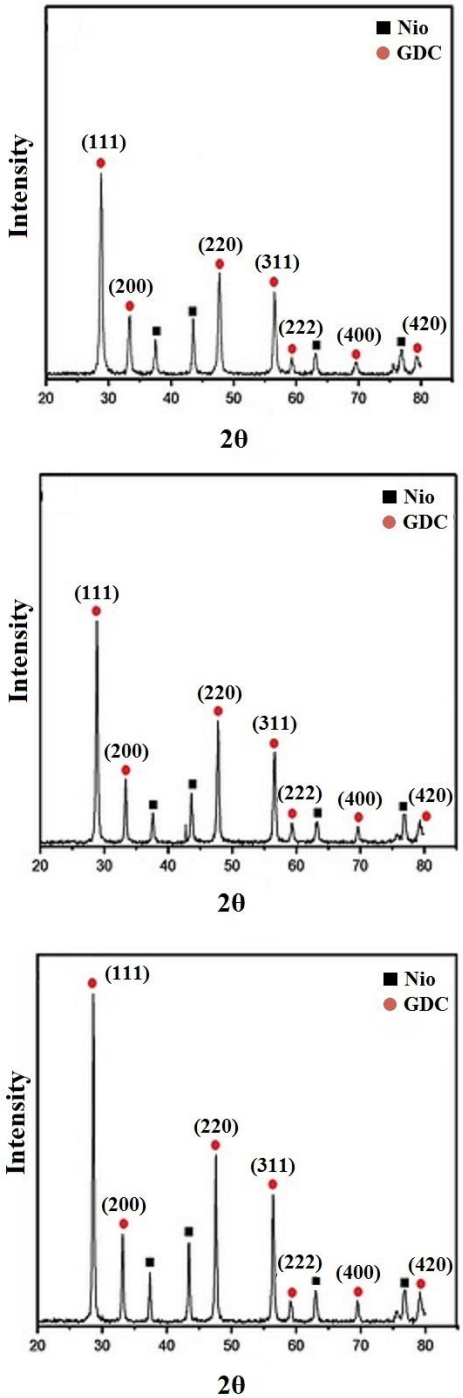

Fig. 7. The X-ray powder diffraction pattern of the a) NGC (a), b) NGC (b) and c) NGC (c)

by the Scherrer equation (Table 2). Considering all the produced NGC powders, the crystallite size of the GDC is smaller than that of NiO. With regard to the temperature variations of NiO and GDC formation, the crystallite size of NiO in all the treatments was higher than GDC [5]. According to the sharp peaks observed in NGC (c) (Fig. 7c), it also becomes clear that the crystallite size values between NiO and GDC phases in NGC (c) powder are higher than those of NGC (a) and NGC (b)

Table 2. The Crystallite sizes of NiO and GDC phases in NGC (a), NGC (b) and NGC (c) powders

Average crystallinity size / nm	NiO	GDC
NGC (a)	71.486	48.25
NGC (b)	47.629	48.25
NGC (c)	35.734	28.80

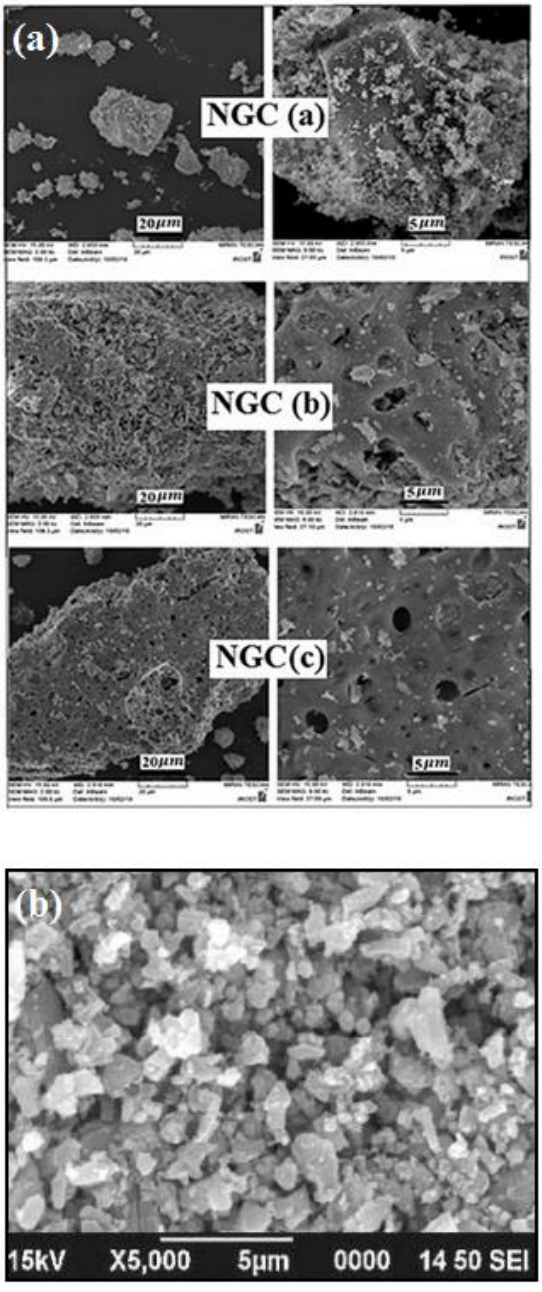

Fig. 8. SEM micrograph of the a) NGC (a), b) NGC (b) and c) NGC (c)

(Fig. 7a, b). SEM analysis revealed the dependence of the morphology of calcined NGC powders on the primary applied Ni complexes, as shown in Fig. 8a. The two phases (NiO and GDC) in the samples are uniformly distributed and well-connected which is favorable for anodic reactions. Additionally,

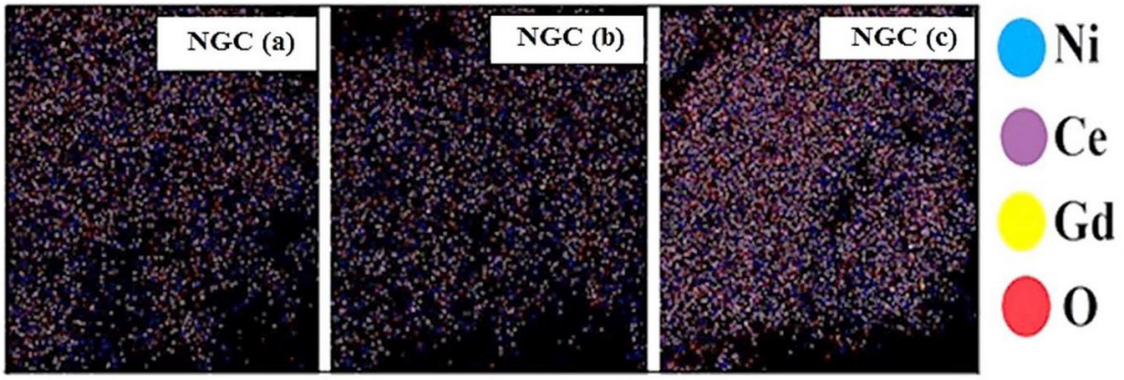

Fig. 9. SEM-EDS mapping of the a) NGC (a), b) NGC (b) and c) NGC (c)

more porous surface with increased pore size and low density is observed for NGC (c) ceramic powder compared to NGC (a) and NGC (b). Since the electrode performance is highly dependent on the microstructure [22], it seems that ionic conductivity in the anodic powder of NGC (c) was higher than those of NGC (a) and NGC (b) due to more porosity and TPB. The SEM of NiO nanoparticles is shown in Fig. 8b [23]. Here, it is clear that the particles were highly agglomerated in nature [23]. Comparing the SEM images of a and b demonstrates that the distribution of NiO in GDC matrix is completely uniform in the NGC composites. In addition, it could be seen that the SEM images of NiO nanoparticles greatly differ from the SEM images of NGC powders. The Distribution pattern of Ni, Ce, and Gd elements in the NGC anode samples was examined by SEM-EDS mapping (Fig. 9). Regarding Fig. 9, it is clear that the homogeneous distribution of the elements in NGC (c) powder is higher than those of NGC (a) and NGC (b). Therefore, the sol-gel method is an effective way to yield fine powders with uniform distribution of elements. The BET test measured the specific surface area of the manufactured NGC samples as well as their pore volume, which is interrelated to the triple-phase boundary. Based on the BET analysis, the NGC (c) powder had the largest specific surface area (82.899 m^2/g) and the average pore volume was approximately 30.825 nm, while the NGC (a) and NGC (b) powders exhibited the specific surface areas of 65.0524, and 76.279 m^2/g and average pore volumes of 17.297 and 22.038 nm, respectively. Larger pore size is suitable for gas phase transport through the pores of NGC powders; however, the non-uniform and smaller pore structure acts as a barrier for gas transport through the pores [11]. The Nyquist impedance plot and the corresponding fitting curve of each symmetrical half-cell for NGC anodes are illustrated in Fig. 10. The width impedance arc on the real axis refers to the polarization resistance (Ep) of the electrodes. According to the Nyquist plot (Fig. 10), it is clear that temperature had a considerable effect on the resistance of samples. By increasing temperature, due to the quick reaction kinetics and increased ionic and electronic conductivity, the resistance level decreased. M.K. Rath et al. [24] proposed that H_2 oxidation on the NiO–GDC system generally induces charge-transfer at the TPB, gas diffusion, dissociation/adsorption of H_2, surface diffusion of the adsorbed species into the TPB, and a conversion. According to the Nyquist plot (Fig. 10), it is clear that the overall performance and electrical properties are directly related to the microstructure of the anode material. This information suggests that proper modification increases the electrochemical activity of NGC (c) cermet anodes for the H_2 oxidation reaction at the electrode-electrolyte interface. Thus, the modification of morphology with increased porosity, active sites at the TPB region, and particle size reduction will boost the activity of NiO/GDC cermet anodes. The polarization resistance (0.106 $\Omega.cm^2$) was lowest in the half-cell with NGC (c) anode powder at 800 °C. Increasing the polarization resistance of NGC (a) (0.8 $\Omega.cm^2$) and NGC (b) (0.65 $\Omega.cm^2$) is likely due to particle coarsening during heat treatment and reduction of the catalytic surface and blockage of active sites of the electrode [1]. Table 3 describes a brief overview of the properties of modified NiO/GDC powders

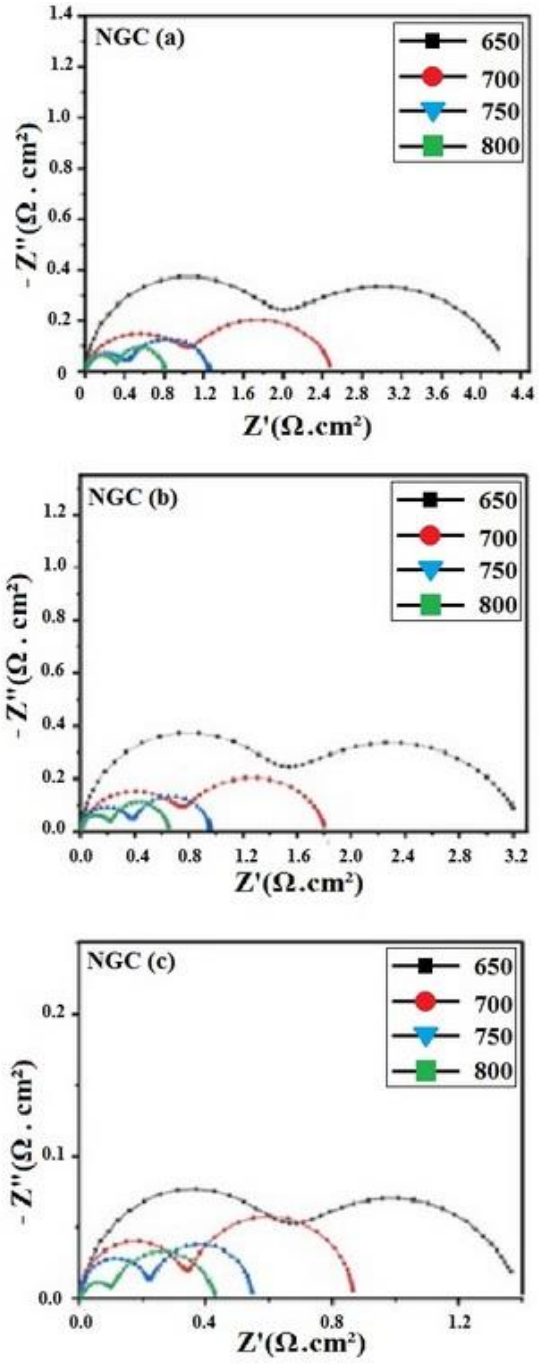

Fig. 10. Polarization resistance values determined at the temperature of 650-800for the a) NGC (a), b) NGC (b) and c) NGC (c)

synthesized by different methods along with their results. The activation energy of the electrode polarization resistance was measured according to the slope of the Arrhenius plots. The activation energy (Ea) and polarization resistance ($\Omega.cm^2$) of NGC (a), (b) and (c) were measured at 650-800 °C and values are presented in Table 4. Moreover, Fig. 11 demonstrates that the NGC (c) sample had the lowest activation energy among NGC (a) and NGC (b). The results presented in Fig. 11 indicate that the modification of the precursors used in the anode synthesis strikingly minimized the

Table 3. A brief overview of the properties of modified NiO/GDC powders synthesized by different methods and their results

Anode material	Type of optimization	Result	Reference
NiO-GDC	Synthesis of NiO-GDC with Nickel varying from 50 to 65 wt.% by conventional solid-state reaction method	Increasing the conductivity of anodic powder with NiO-GDC ratio (65-35) compared to the NiO -YSZ ratio (50-50) at 973 K	[25]
NiO-GDC	Using sodium alginate as the templating material for the synthesis of NiO-GDC	Reduce polarization resistance at low operating temperature by increasing porosity and surface area	[26]
NiO-GDC-YSZ	Use of the mixture of GDC and YSZ phases for physical and conductivity evaluation	Change of ohmic resistance and polarization	[27]
NiO-GDC	Doping of copper in anode materials	Decrease the carbon deposition and enhance the performance of SOFC at low temperature	[28]
Ni-GDC/Ni-SDC	Use of a modified citrate-nitrate combustion method for synthesis	High electrical conductivity	[29]
Ni/10Sc1CeSZ	Use of a microwave-assisted glycine nitrate combustion process for synthesis	The improved performance and morphology of cermet powder	[30]

Table 4. The activation energy (Ea) and polarization resistance ($\Omega.cm^2$) of NGC (a), NGC (b) and NGC (c) at 650-800 °C

Sample	Polarization resistance / $\Omega.cm^2$	Activation energy / E_a
NGC (a)	0.8	0.94
NGC (b)	0.65	0.90
NGC (c)	0.106	0.69

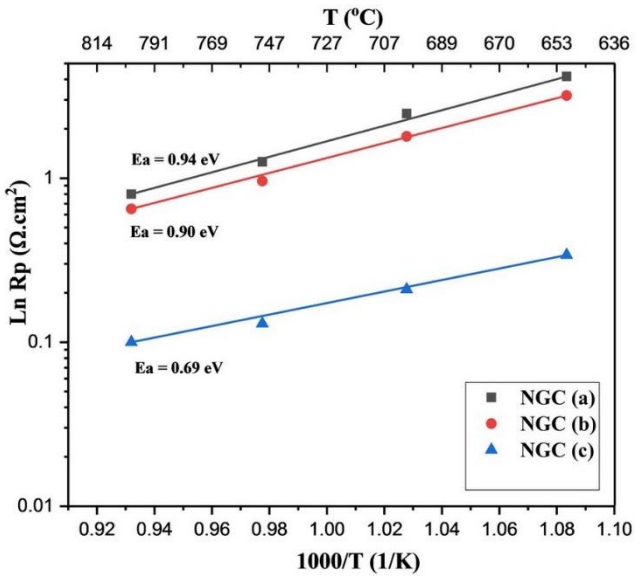

Fig. 11. Activation energy of the a) NGC (a), b) NGC (b) and c) NGC (c)

composites' activation energy. In fact, good morphology and pore size distribution of the NGC (c) sample had a desirable effect on lowering the polarization resistance and activation energy. Overall, this method may be considered as a replacement for NiO/GDC anode agents synthesized with nickel nitrate salt for intermediate SOFCs.

CONCLUSION

To analyze the influence of precursors on microstructure and electrical conductivity, NiO-GDC anode powders with different Nickel(II) coordination compounds as precursors were successfully obtained by applying the sol-gel method. The results demonstrated that a more porous structure, high surface area and higher TPB for the NGC (c) anode was obtained. IES analysis of the NiO/GDC anodes confirmed that the polarization resistance for H_2 oxidation depends significantly on the microstructure of the NiO/GDCs. The NGC (c) composed of $[NiL^2(\mu\text{-}2,6\ pyridinedicarboxylate)]_n$ revealed the best electrocatalytic activity in the solid oxide fuel cell operating circumstances.

CONFLICTS OF INTEREST

The authors announce that there are no conflicts of interest.

REFERENCES

1. Rafique M, Nawaz H, Shahid Rafique M, Bilal Tahir M, Nabi G, Khalid NR. Material and method selection for efficient solid oxide fuel cell anode: Recent advancements and reviews. International Journal of Energy Research. 2018;43(7):2423-46.
2. Araújo AJM, Grilo JPF, Loureiro FJA, Campos LFA, Paskocimas CA, Nascimento RM, et al. Designing experiments for the preparation of Ni-GDC cermets with controlled porosity as SOFC anode materials: effects on the electrical properties. Ceramics International. 2018;44(18):23088-93.
3. Zha S, Moore A, Abernathy H, Liu M. GDC-Based Low-Temperature SOFCs Powered by Hydrocarbon Fuels. Journal of The Electrochemical Society. 2004;151(8):A1128.
4. Ishihara.T ST, Nishiguchi. H, Takita. Y. Nickel – Gd-doped CeO_2 cermet anode for intermediate temperature operating solid oxide fuel cells using $LaGaO_3$-based perovskite electrolyte. Solid State Ionics. 2000;132(3-4):209-16.
5. Sharma V, Liu Q, Crozier P, Sharma R. In Situ Nanostructural Changes in Ni-GDC Anode for Solid Oxide Fuel Cells Observed Using an Environmental Transmission Electron Microscope. Microscopy and Microanalysis. 2012;18(S2):1128-9.
6. Fergus J. Oxide anode materials for solid oxide fuel cells. Solid State Ionics. 2006;177(17-18):1529-41.
7. Shimada H, Takami E, Takizawa K, Hagiwara A, Ihara M. Highly dispersed anodes for solid oxide fuel cells using NiO/YSZ/BZY triple-phase composite powders prepared by spray pyrolysis. Solid State Ionics. 2011;193(1):43-51.
8. Liu Z, Liu B, Ding D, Liu M, Chen F, Xia C. Fabrication and modification of solid oxide fuel cell anodes via wet impregnation/infiltration technique. Journal of Power Sources. 2013;237:243-59.
9. Razpotnik T, Marinšek M, Novosel B, Zupan K, Francetič V, Maček J. A polymer complex solution process for the synthesis and characterization of Ni–YSZ cermet material. Ceramics International. 2008;34(7):1741-6.
10. Yoon SP, Han J, Nam SW, Lim T-H, Hong S-A. Improvement of anode performance by surface modification for solid oxide fuel cell running on hydrocarbon fuel. Journal of Power Sources. 2004;136(1):30-6.
11. Prakash BS, Pavitra R, Kumar SS, Aruna ST. Evaluation of solution combustion synthesized NiO/GDC ceramic powders for anode substrate and anode functional layers of intermediate temperature solid oxide fuel cell. Ceramics International. 2017;43(15):12138-44.
12. Pezeshkpour S, Salamatinia B, Amini Horri B. Synthesis and characterization of nanocrystalline NiO-GDC via sodium alginate-mediated ionic sol-gel method. Ceramics International. 2018;44(3):3201-10.
13. Soltanianfard MJ, Esmaielzadeh S, Parsam S, Rahmani Nejad A. Hydrothermal synthesis of copper(II) and Nickel(II) nano complexes with unsymmetric tetradentate Schiff base ligand. New precursors for preparation of copper(II) and nickel(II) oxides nano-particles. Nanochemistry Research. 2018;3(2):197-204.
14. Ghamari S, Ranjbar M, Nabitabar M. Preparation and characterization of nanopowder nickel oxide/gadolinium-doped ceria via the sol-gel method by NiLH2 precursor. Journal of Sol-Gel Science and Technology. 2016;81(1):236-46.
15. Ni W-X, Li M, Zhan S-Z, Hou J-Z, Li D. In Situ Immobilization of Metalloligands: A Synthetic Route to Homometallic Mixed-Valence Coordination Polymers. Inorganic Chemistry. 2009;48(4):1433-41.
16. Babaei A, Jiang SP, Li J. Electrocatalytic Promotion of Palladium Nanoparticles on Hydrogen Oxidation on Ni/GDC Anodes of SOFCs via Spillover. Journal of The Electrochemical Society. 2009;156(9):B1022.
17. Palacios EG, Juárez-López G, Monhemius AJ. Infrared spectroscopy of metal carboxylates. Hydrometallurgy. 2004;72(1-2):139-48.
18. Mehrotra. R.C BR. Metal Carboxylates. London, UK: AcademicPress; 1983.
19. Zarkov A, Stanulis A, Salkus T, Kezionis A, Jasulaitiene V, Ramanauskas R, et al. Synthesis of nanocrystalline gadolinium doped ceria via sol–gel combustion and sol–gel synthesis routes. Ceramics International. 2016;42(3):3972-88.
20. Chourashiya MG, Jadhav LD. Synthesis and characterization of 10%Gd doped ceria (GDC) deposited on NiO-GDC anode-grade-ceramic substrate as half cell for IT-SOFC. International Journal of Hydrogen Energy. 2011;36(22):14984-95.
21. Prasad DH, Son JW, Kim BK, Lee HW, Lee JH. Synthesis of nano-crystalline Ce0.9Gd0.1O1.95 electrolyte by novel sol–gel thermolysis process for IT-SOFCs. Journal of the European Ceramic Society. 2008;28(16):3107-12.
22. Grilo JPF, Moura CG, Macedo DA, Rajesh S, Figueiredo FML, Marques FMB, et al. Effect of composition on the

structural development and electrical conductivity of NiO-GDC composites obtained by one-step synthesis. Ceramics International. 2017;43(12):8905-11.
23. Sagadevan S, Podder J. Investigations on structural, optical, morphological and electrical properties of nickel oxide nanoparticles. International Journal of Nanoparticles. 2015;8(3/4):289.
24. Rath MK, Sahoo T, Lee K-T. Catalytic activity of morphology-tailored NiO–Ce0.8Gd0.2O2–δ synthesized by a hexamethylenetetramine (HMT)-assisted solvothermal process. Ceramics International. 2015;41(10):12742-50.
25. Soman AK, Kuppusami P, Rabel AM. Electrical Conductivity of NiO-Gadolinia Doped Ceria Anode Material for Intermediate Temperature Solid Oxide Fuel Cells. Nano Hybrids and Composites. 2017;17:224-36.
26. Choo CK, Horri BA, Salamatinia B, editors. Synthesis and characterization of nickel(II) oxide/gadolinium-doped ceria (NiO/GDC) nanocomposites as a potential material for anode supported LT-SOFCs. Proceedings of the World Congress on Engineering and Computer Science; 2016.
27. Lenser C, Jeong H, Sohn YJ, Russner N, Guillon O, Menzler NH. Interaction of a ceria-based anode functional layer with a stabilized zirconia electrolyte: Considerations from a materials perspective. Journal of the American Ceramic Society. 2017;101(2):739-48.
28. Jeon OS, Lee JG, Ji Y, Lee S-h, Kwon O, Kim JP, et al. Effects of dispersed copper nanoparticles on Ni-ceria based dry methanol fuelled low temperature solid oxide fuel cells. RSC Advances. 2019;9(11):6320-7.
29. Skalar T, Zupan K, Marinšek M. Microstructure tailoring of combustion-derived Ni-GDC and Ni-SDC composites as anode materials for intermediate temperature solid oxide fuel cells. Journal of the Australian Ceramic Society. 2018;55(1):123-33.
30. Jais AA, Ali SAM, Anwar M, Somalu MR, Muchtar A, Isahak WNRW, et al. Performance of Ni/10Sc1CeSZ anode synthesized by glycine nitrate process assisted by microwave heating in a solid oxide fuel cell fueled with hydrogen or methane. Journal of Solid State Electrochemistry. 2020;24(3):711-22.